Newton

Article

Smith-Purcell radiation from time grating

Graphical abstract

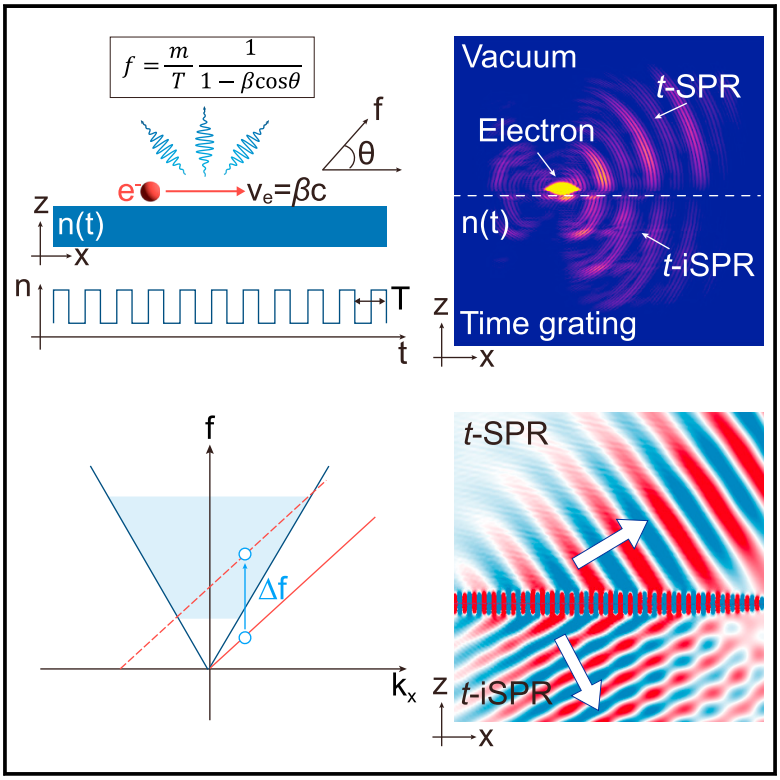

Highlights

- Derived a generalized dispersion equation for temporal Smith-Purcell radiation
- Demonstrated the phenomenon through proof-of-principle simulations
- Highlighted the differences between spatial and temporal Smith-Purcell radiation
- Proposed potential experiments for future implementation

Authors

Juan-Feng Zhu, Ayan Nussupbekov, Yudi Fan, ..., Ching Eng Png, Cheng-Wei Qiu, Lin Wu

Correspondence

chengwei.qiu@nus.edu.sg (C.-W.Q.), lin_wu@sutd.edu.sg (L.W.)

In brief

Electrons moving across a spatially periodic grating emit Smith-Purcell radiation, a phenomenon widely used in applications such as particle accelerators and free-electron lasers. Zhu et al. demonstrate through computational methods that Smith-Purcell radiation can also be generated in time-varying, spatially invariant structures. This approach offers a more robust and versatile platform for producing free-electron light emission.

Zhu et al., 2025, Newton *1*, 100023
April 7, 2025
https://doi.org/10.1016/j.newton.2025.100023

CellPress

Newton

CellPress
OPEN ACCESS

Article

Smith-Purcell radiation from time grating

Juan-Feng Zhu,[1] Ayan Nussupbekov,[2] Yudi Fan,[1] Wenjie Zhou,[1,3] Zicheng Song,[4] Xuchen Wang,[5] Zi-Wen Zhang,[6] Chao-Hai Du,[6] Xianlong Wei,[7] Ping Bai,[2] Ching Eng Png,[2] Cheng-Wei Qiu,[3,*] and Lin Wu[1,2,8,*]

[1]Science, Mathematics and Technology, Singapore University of Technology and Design, 8 Somapah Road, Singapore 487372, Singapore
[2]Institute of High Performance Computing, Agency for Science, Technology, and Research (A*STAR), 1 Fusionopolis Way, #16-16 Connexis, Singapore 138632, Singapore
[3]Department of Electrical and Computer Engineering, National University of Singapore, 4 Engineering Drive 3, Singapore 117583, Singapore
[4]Center for Composite Materials and Structures, School of Astronautics, Harbin Institute of Technology, Harbin, China
[5]Institute of Nanotechnology, Karlsruhe Institute of Technology, Karlsruhe, Germany
[6]Optical Communication Systems and Networks, School of Electronics, Peking University, Beijing, China
[7]Key Laboratory for the Physics and Chemistry of Nanodevices, School of Electronics, Peking University, Beijing, China
[8]Lead contact
*Correspondence: chengwei.qiu@nus.edu.sg (C.-W.Q.), lin_wu@sutd.edu.sg (L.W.)
https://doi.org/10.1016/j.newton.2025.100023

ACCESSIBLE OVERVIEW Smith-Purcell radiation is emitted when an electron traverses a spatially periodic grating and has found diverse applications in areas such as particle accelerators and free-electron lasers. This work investigates theoretically and computationally how the phenomenon can be similarly achieved in structures that vary periodically in time and provides suggestions for experimental implementation. The use of temporally instead of spatially periodic variation boosts light emission and provides a more robust and versatile means of producing free-electron radiation. This advancement holds promise for developing advanced on-chip light sources and also fosters the progress of time-varying materials and applications.

SUMMARY

Smith-Purcell radiation (SPR) arises when an electron moves above a spatial grating, where fixed momentum compensation constrains the emission wavelength. In contrast, temporal SPR (*t*-SPR) utilizes a time grating to leverage temporal periodicity for energy compensation, enabling more flexible radiation control. We introduce a generalized dispersion equation for *t*-SPR that predicts the interplay between radiation frequency, direction, electron velocity, modulation period, and harmonic orders. *t*-SPR offers several advantages over conventional SPR: robustness (*t*-SPR maintains stable emission intensity without rapid decay as the electron moves away from the time grating), versatility (*t*-SPR enables precise control via temporal modulation of period, amplitude, and waveform), and amplified emission (temporal modulation introduces additional energy channels, boosting emission). These features make *t*-SPR highly promising for advanced applications in on-chip light sources and electron accelerators.

INTRODUCTION

Smith-Purcell radiation (SPR) originates when fast-moving charged particles traverse above a spatially periodic grating, a phenomenon first explained by D.H. Smith and E.M. Purcell.[1] Over the years, SPR has found diverse applications in vacuum electronic devices,[2] particle accelerators,[3] and free-electron lasers.[4] Recent advances in SPR have leveraged metamaterials,[5,6] enabling precise control over coherence, polarization, and radiation direction.[7–13] Captivating optical phenomena such as bound states in the continuum[14] and flat-band resonances[15] have been harnessed to significantly enhance the intensity of SPR. However, state-of-the-art research on SPR continues to rely on "momentum compensation" facilitated by spatial modulations in time-invariant designs, emphasizing the manipulation of SPR emission through photonic structures.

A special class of metamaterials, known as time-varying metamaterials, introduces a dynamic aspect by altering their physical properties over time, offering new dimensions for manipulating light waves beyond traditional spatial control.[16–22] When these metamaterials undergo sudden changes in their electromagnetic properties, they create temporal boundaries where momentum, rather than energy, is conserved due to spatial translational invariance.[21,22] Early forms of time-varying metamaterials date back to the 1970s, where acoustic wave modulation of the refractive index led to observations of novel transition radiation peaks when electrons encountered such non-stationary boundaries.[23–28] Modern applications have expanded significantly, encompassing time

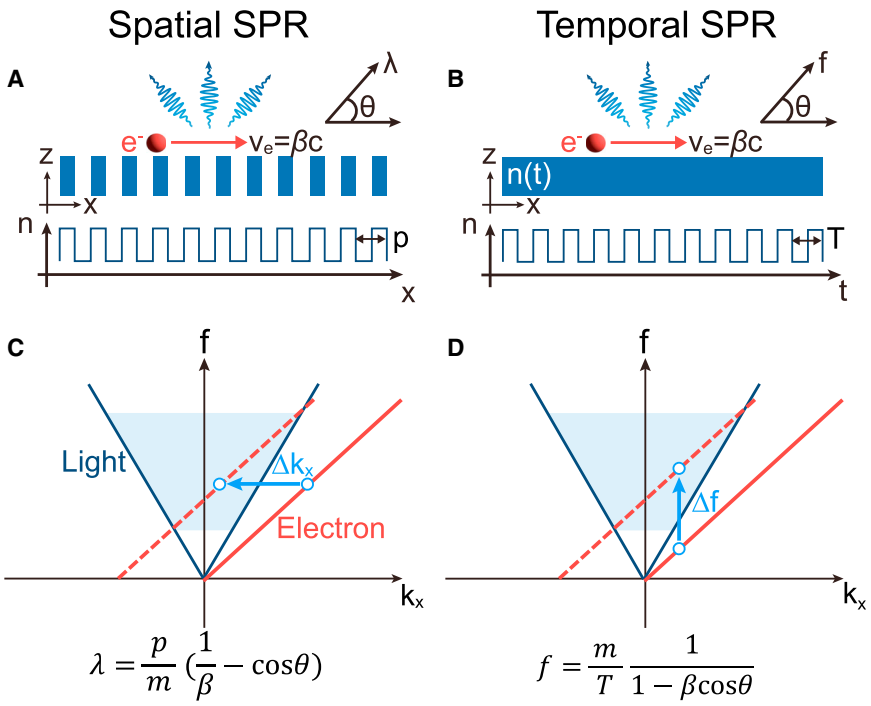

Figure 1. Schematics of *s*-SPR and *t*-SPR

(A and B) Two-dimensional (2D) models in the x-z plane are illustrated for cases where a swift free electron (i.e., source electron) travels above (A) a grating with period p or (B) a time grating with period T.

(C and D) Dispersion diagrams for (C) *s*-SPR and (D) *t*-SPR show the light cone in vacuum (blue lines) and source electron dispersion curve (red solid lines), which shifts left/right along the k_x axis for *s*-SPR and upward/downward along the f axis for *t*-SPR. The radiation wavelength (or frequency) of *s*-SPR and *t*-SPR are determined by the normalized electron velocity $(\beta = v_e/c)$ and modulation period (p or T).

reversal,[29] nonreciprocity,[30,31] temporal aiming,[32] quantum physics,[33] and other emerging possibilities.[34–41] Of particular interest is the concept of photonic time crystals, which are created through periodic temporal modulation, resulting in momentum bands and gaps.[42] This has revealed the intriguing phenomenon of exponential energy growth within momentum gaps, offering pathways to achieve light amplification.[43,44] Importantly, the periodic temporal modulation induces frequency harmonic waves rather than momentum harmonic waves, providing a versatile platform for manipulating light.[18–20,45,46] For example, waves propagating through a time grating (TG) can couple to near-field surface waves via frequency down-conversion.[45] Furthermore, temporal modulation enhances energy transfer, allowing free electrons to induce radiation within photonic time crystals with energy below conventional thresholds.[46]

Inspired by seminal works on electron-induced radiation[23–28] in photonic time crystals,[46] we introduce the concept of temporal SPR (*t*-SPR) originating from a TG, akin to conventional spatial SPR (*s*-SPR) from a grating. As the electron traverses above the TG, *t*-SPR can be stimulated across a wide frequency spectrum. In this study, we aim to extend the foundational principles of *s*-SPR to *t*-SPR. We begin by deriving the *t*-SPR dispersion equation, elucidating the interplay between radiation frequency f, radiation direction θ, normalized electron velocity β, and harmonic order m. Subsequently, we employ full-wave electromagnetic simulations to validate our theoretical framework. To tailor the characteristics of *t*-SPR compared to *s*-SPR, we investigate optimal conditions for maximizing its radiation intensity. This exploration encompasses internal factors such as electron-grating separation d and normalized electron velocity β, as well as external factors like the temporal modulation function and amplitude. Our endeavor aims to pave the way for a new frontier in research: developing "active" free-electron light sources enabled by temporal modulation, surpassing the capabilities of conventional spatial methods.

RESULTS

Analytical dispersion equations

Our two-dimensional (2D) model, illustrated in Figure 1, is situated in the x-z plane, with a free electron (i.e., source electron) moving at velocity $v_e = \beta c$ along the x direction, where c is the speed of light in vacuum. The momentum-frequency dispersion diagram in Figure 1C illustrates the mechanism of *s*-SPR, which is depicted in Figure 1A. The blue line represents the light cone $\omega_{light} = ck_0$, where ω_{light} (or k_0) is the angular frequency (or wavenumber) of light in vacuum. The dispersion relation of the source electron can be expressed as $\omega_e = 2\pi f_e = v_e k_{xe}$ (red solid line), where ω_e (f_e, or k_{xe}) is the angular frequency (frequency, or propagation wavenumber along the x axis) of the source electron. Given $v_e < c$, it follows that $k_{xe} > k_0$, indicating that the electromagnetic wave carried by the source electron is evanescent. The spatial grating (with grating period p) compensates the source electron's momentum with $\Delta k_x = 2\pi m/p$, where m denotes the diffraction order. Consequently, the electron dispersion curve shifts along the k_x axis, as indicated by the blue arrow in Figure 1C. When the electron dispersion curve shifts above the light cone (red dashed line), the evanescent wave can diffract into a propagating wave in a vacuum. The corresponding radiation frequency range is determined by the intersection points between the electron dispersion curve and the light cone (blue region). The SPR dispersion relation is obtained through momentum-matching conditions:

$$\lambda = \frac{p}{m}\left(\frac{1}{\beta} - \cos\theta\right). \qquad \text{(Equation 1)}$$

On the other hand, when the properties of the materials, e.g., refractive index n, periodically vary with respect to time rather than space, a TG is created, as shown in Figure 1B. According to the Bloch-Floquet theorem, the electric field of TG can be

expanded using a Fourier series representation, $E(t) = \sum_m e_m e^{j(\omega_e + m\Omega)t}$, where $\Omega = 2\pi f_m$ and $f_m = 1/T$ represents the modulation frequency, with T being the modulation period. Here, m ranges over $0, \pm 1, \pm 2, \cdots$, denoting harmonic orders, and e_m denotes the coefficient associated with the m^{th} harmonic order. This formula immediately implies that temporal modulation induces frequency harmonics.[47] When the source electron hovers above TG (grating/free-space interface at $z = 0$) with a separation distance d, the excitation of the source electron is given by $\mathbf{J}(x,z,t) = \hat{\mathbf{x}} q v_e \delta(z - d)\delta(x - v_e t)$, where q is the elementary charge. The frequency domain expression is obtained through Fourier transform $\mathbf{J}(x,z,\omega) = \hat{\mathbf{x}} q \delta(z - d) e^{-jk_{xe}x}$. Hence, the evanescent wave induced by the source electron can be written as[48]

$$\mathbf{H}_y^i(x,z,t) = -\hat{\mathbf{y}}\frac{q}{2}\mathrm{sgn}(z-d)e^{j\omega_e t}e^{-jk_{xe}x - jk_{z0}|z-d|}, \quad \text{(Equation 2)}$$

$$\mathbf{E}_x^i(x,z,t) = -\hat{\mathbf{x}}\frac{q}{2}\frac{k_{z0}}{\omega\varepsilon_0}e^{j\omega_e t}e^{-jk_{xe}x - jk_{z0}|z-d|}, \quad \text{(Equation 3)}$$

where k_{z0} indicates the wavenumber of the source electron in the z direction with harmonic order $m = 0$ and $k_{xe}^2 + k_{z0}^2 = (\omega_e/c)^2$. With the frequency harmonic components introduced by TG, the reflected wave in vacuum $(z > 0)$ is

$$\mathbf{H}_y^r(x,z,t) = \hat{\mathbf{y}}\sum_m R_m e^{j(\omega_e + m\Omega)t}e^{-jk_{xe}x - jk_{zm}z}, \quad \text{(Equation 4)}$$

$$\mathbf{E}_x^r(x,z,t) = \hat{\mathbf{x}}\sum_m R_m \frac{k_{zm}}{(\omega_e + m\Omega)\varepsilon_0}e^{j(\omega_e + m\Omega)t}e^{-jk_{xe}x - jk_{zm}z}, \quad \text{(Equation 5)}$$

where $k_{xe}^2 + k_{zm}^2 = [(\omega_e + m\Omega)/c]^2$, and R_m represents the reflection coefficient of the m^{th} harmonic wave. Based on Equations 4 and 5, the electron dispersion line shifts either upward $(m > 0)$ or downward $(m < 0)$ along the f axis in Figure 1D, reflecting the change in the source electron's energy induced by the TG. Likewise, when the electron dispersion line moves above the light cone, the evanescent wave is converted into the plane wave and gives rise to the t-SPR at radiation frequency $\omega = 2\pi f$, where $\omega = \omega_e + m\Omega$. The corresponding dispersion equation can be expressed as follows (see Note S1 for derivation):

$$f = \frac{m}{T}\frac{1}{1 - \beta\cos\theta}. \quad \text{(Equation 6)}$$

The same t-SPR dispersion equation can be obtained by replacing the grating period p with Tv_e in the s-SPR dispersion equation. It reveals that the frequency of t-SPR can be customized by T and spans a frequency band for the m^{th} frequency harmonic wave:

$$\frac{m}{1+\beta}\frac{1}{T} < f < \frac{m}{1-\beta}\frac{1}{T}. \quad \text{(Equation 7)}$$

Numerical simulations of t-SPR

To validate this dispersion relation, we conducted numerical simulations of t-SPR, aiming to reveal key characteristics as illustrated in Figure 2. The simulations utilized a 2D time-domain solver within COMSOL Multiphysics, which solves Maxwell's equations discretized in both space and time (see methods, Note S2, and Figure S1). Each moving electron was modeled as a series of electric point dipoles with phase delays determined by electron velocity β.[14,15,49,50] We set our refractive index modulation function as $n(t) = A \cdot W(t) + n_a$, where A denotes the amplitude, $W(t)$ represents the modulation waveform, and n_a is the central refractive index. The following parameters are used throughout this study unless stated otherwise: $A = 0.2$, $n_a = 1.5$, $f_m = 20$ GHz, W is in an ideal square waveform, $\beta = 0.2$, and $d = 0.5$ mm. This work is theoretical and imposes no constraints on modulation, with the chosen parameters being feasible in systems such as graphene plasmonics.[51] Subsequent investigations will look into parameter selection and potential experimental connections, which will be explored in detail in forthcoming discussions.

As shown in Figure 2A, when the electron flies over the TG, it generates radiation both within the vacuum and within the TG. Upon removing the temporal modulation, both radiations become imperceptible, indicating the crucial role played by temporal modulation. To gain insight into the underlying mechanisms, we plot the dispersion diagram in Figure 2B. Here, the dispersion curve of TG (orange line) is derived by matching the temporal boundaries, which exhibits momentum gaps occurring at integer multiple frequencies of $0.5f_m$ (see methods, Note S3, and Figure S2). Within the momentum gap, the wave experiences exponential growth over time.[42,43,46] The asymptotic light line in TG can also be expressed as $\omega_{\text{TG}} = ck_x/n_{\text{eff}}$, with n_{eff} denoting the effective refractive index of TG.[47,52,53] Meanwhile, the frequency harmonic dispersion curve of the source electron shifts either upwards or downwards by an amount of mf_m along the f axis. For example, the case of $m = 1$ is considered (red dashed); this 1st harmonic wave transits above the light cone, generating an overlapping area depicted as the blue region. It indicates the conversion of the evanescent wave into a propagating wave, thereby giving rise to t-SPR. Simultaneously, this 1st harmonic wave reaches above the TG light cone, leading to an overlapping area depicted as the gray region, indicating conversion into a propagating plane wave into TG. The radiation induced within the TG, driven by energy compensation from the temporal modulation, is a type of Floquet diffraction radiation. This phenomenon, similar to diffraction radiation in spatially periodic systems,[54] can be referred to as temporal internal SPR (t-iSPR).

Figure 2C presents the simulated radiation spectrum. As the TG shifts the electron harmonic line upward along the f axis, the radiation characteristics at the radiation frequency f rely on the source electron at the frequency $f_e = f - mf_m$, whose evanescent field decays exponentially with transverse distance from its axis of motion. Quantitatively, the decay distance increases as the frequency f_e decreases while maintaining a constant velocity, according to the Bohr cutoff

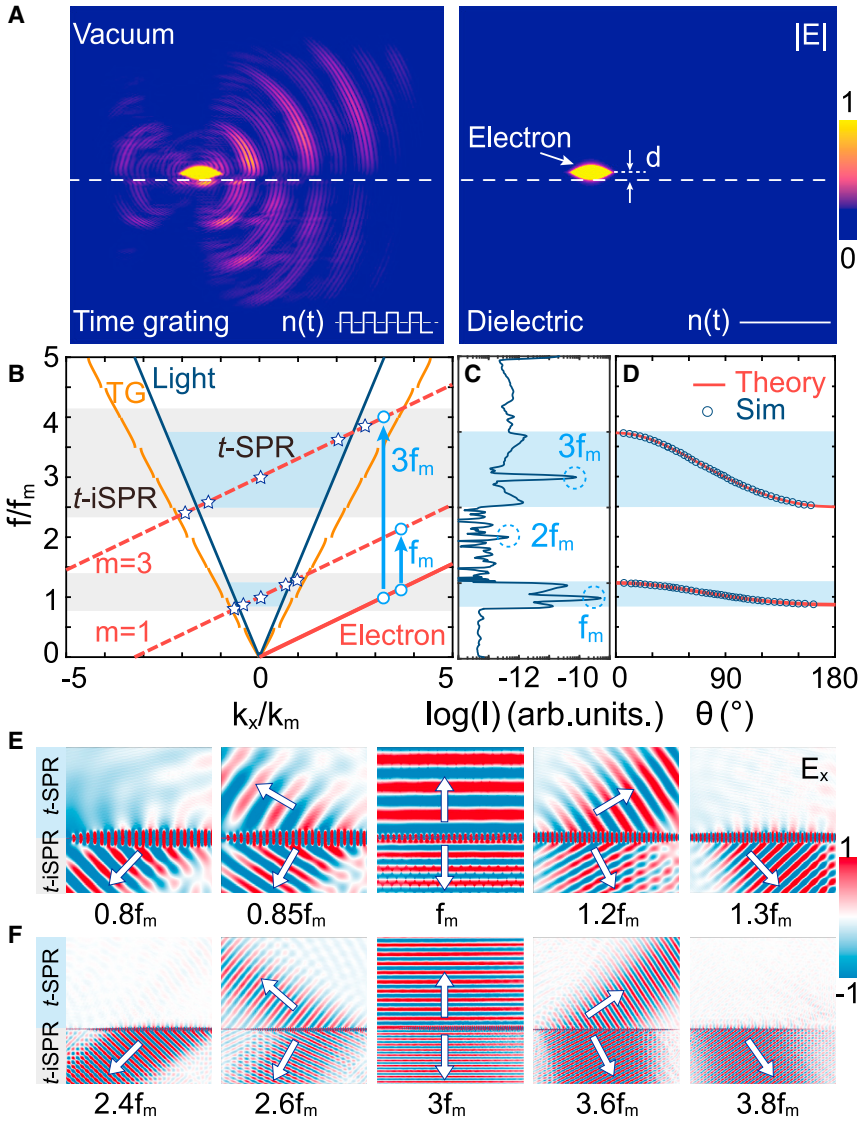

Figure 2. Proof-of-principle simulations of *t*-SPR in an exemplified system with $\beta = 0.2$ and $f_m = 20$ GHz

(A) Electric field intensity profiles when a source electron flies over a dielectric slab with or without a temporal modulation.

(B) The dispersion diagram of the exemplified system: light line (dark blue), energy band within TG (orange), electron (solid red), electron harmonic wave (dashed red), the radiation frequency range for *t*-SPR (blue regions), and *t*-iSPR (gray regions).

(C) *t*-SPR radiation spectrum probed in the vacuum.

(D) Radiation angle (θ) vs. frequency: theory (solid line) and simulations (symbols).

(E and F) Simulated electric field distributions (E_x) at selected frequencies marked by stars in (B) for 1st ($m = 1$) and 3rd ($m = 3$) harmonic orders, where the arrows indicate the radiation directions.

distance[50,55]: $d_{\mathrm{Bohr}}(f_e) = c\beta/(2\pi f_e\sqrt{1-\beta^2})$. The evanescent field interacting with the TG becomes much stronger when f_e approaches zero. Consequently, the radiation intensity peaks at $f = f_m$ and diminishes as f deviates from f_m.

In addition, Equation 6 predicts a relationship between the radiation angle and frequency, which is shown in Figure 2D (line). As suggested, *t*-SPR exhibits a beam-scanning characteristic within the operation bandwidth. The radiation direction switches from backward ($180° \rightarrow 90°$) to forward ($90° \rightarrow 0°$) as f increases, and a normal emission is produced at $f = f_m$. This relationship has been validated by our simulations in Figure 2D (symbols) and vividly illustrated by the electric field distributions in Figure 2E: 0.85 f_m (backward), f_m (normal), and 1.2 f_m (forward). Moreover, *t*-SPR ceases to appear outside the predicted *t*-SPR range ($0.83f_m < f < 1.25f_m$). Here, the simulated electric field distributions encompass both the *t*-SPR emission and the evanescent wave induced by the source electron. The presence of the evanescent wave results in periodic fluctuations in the electric field distribution near the TG.

Interestingly, along with *t*-SPR, *t*-iSPR can also be induced within TG due to the phase velocity of the 1st harmonic wave exceeding that of light within TG, as evidenced in Figure 2B. The frequency range of *t*-iSPR can be divided into two regions by the line $f = f_m$, which manifest themselves in the left ($k_x < 0$) and right ($k_x > 0$) half-spaces, respectively, signifying that the energy flow propagates backward or forward with respect to the motion of the electron. As depicted in Figure 2E, backward *t*-iSPR is evident at 0.8 and $0.85f_m$, while forward *t*-iSPR is observed at 1.2 and $1.3f_m$. This backward radiation effect is similar to reverse Cherenkov radiation, which helps separate electrons from the wakefields they generate, offering a wide range of applications in high-energy particle physics.[56–58] Here, the introduction of *t*-iSPR offers an alternative approach for related applications, offering new possibilities for radiation generation within time-varying media.

The electron energy in our setup ($\beta = 0.2$) is well below the Cherenkov radiation threshold ($\beta_{\mathrm{CR}} = 1/1.7 \approx 0.59$). Periodic temporal modulation provides the necessary energy boost for electrons to induce radiation,[46] offering an alternative to hyperbolic metamaterials.[59] When the electron energy exceeds the minimum threshold within the TG (e.g., $\beta = 0.6$), Cherenkov diffraction radiation[54,60] is induced by the fundamental wave ($m = 0$), as the increased slope allows for direct excitation (see Note S4 and Figure S3). Its intensity is significantly greater than *t*-iSPR, with the radiation direction fixed by the Cherenkov diffraction radiation angle and independent of frequency.

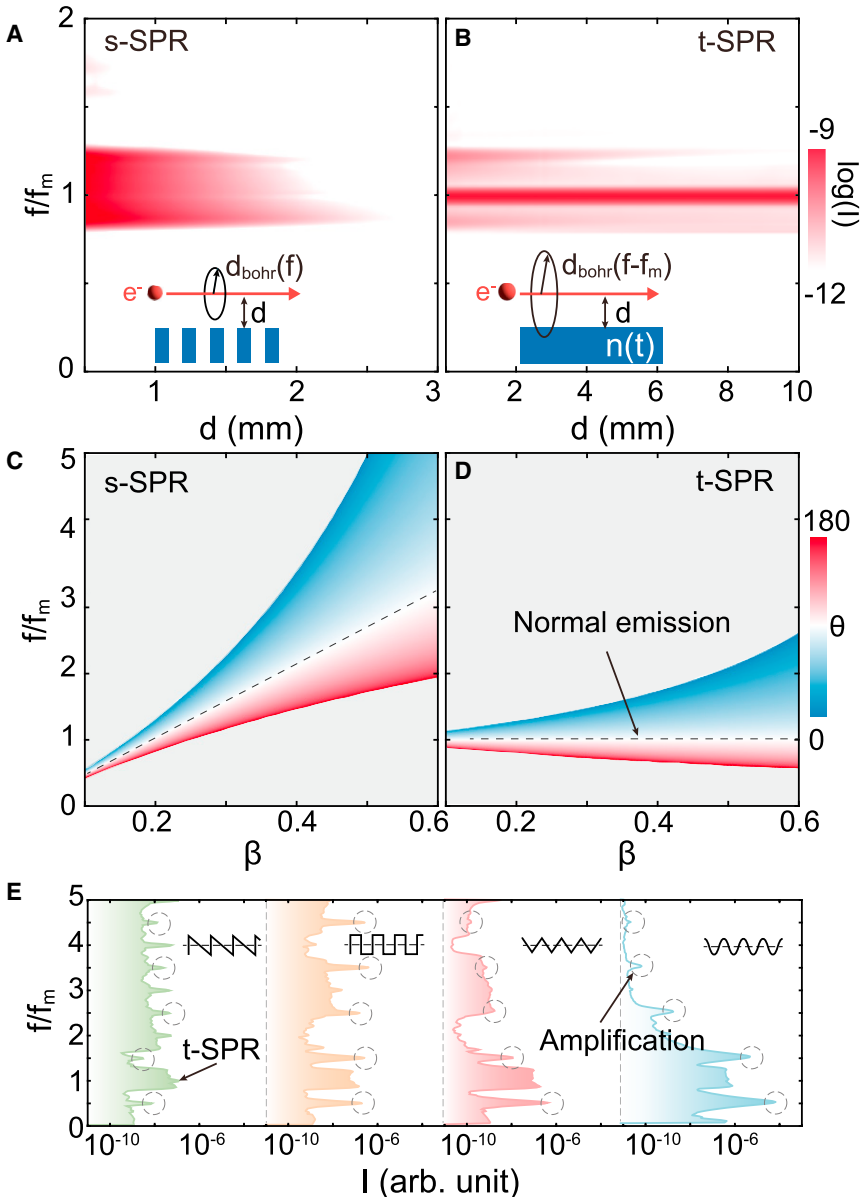

Figure 3. Quantitative analysis for 1st-order *s*-SPR and *t*-SPR

(A and B) The dependence of emission intensity spectra on electron-grating separation d for (A) *s*-SPR or (B) *t*-SPR.

(C and D) Plot of the radiation direction θ as a function of electron velocity β and radiation frequency f for (C) *s*-SPR and (D) *t*-SPR. The gray region indicates angles beyond the 1st-order emission range.

(E) Active control of *t*-SPR via modulation of the continuous waveform $W(t)$, with the amplified peak marked by dashed circles. Adjusting the electron energy to $\beta = 0.23$ positions the interaction within the momentum gap of TG.

Similar to *s*-SPR, *t*-SPR also exhibits high-order harmonic radiation. For example, the 3rd harmonic radiation around $f = 3f_m$ is illustrated in Figure 2B. The radiation angle, observed in numerical simulations, aligns closely with theoretical expectations, as shown in Figure 2D. However, compared to 1st-order radiation, the intensity plotted in Figure 2C is noticeably lower due to the decreasing harmonic intensity with increasing orders.[61,62] This is supported by the electric field distributions around $f = 3f_m$ in Figure 2F, which shows a weaker intensity compared to $f = f_m$ in Figure 2E. Meanwhile, higher-order radiation ($m \geq 3$) overlaps, contributing to the broadband nature of the spectrum. Despite this, *t*-SPR presents a promising pathway for achieving frequency up-conversion and holds potential applications in extreme frequency lasing, particularly in the ultraviolet range.[63] It is noteworthy that the radiation spectrum near $2f_m$ is significantly weaker, as shown in Figure 2C, primarily due to the nature of the Fourier transform of the square modulation waveform. This results in a Sinc function, which causes even harmonics to appear relatively weak.[61]

Quantitative comparisons: *s*-SPR vs. *t*-SPR

In *s*-SPR and *t*-SPR, the conversion of the electron's evanescent wave into free-space radiation is facilitated through the compensation of momentum or energy from the spatial grating or TG, respectively. Their characteristics exhibit several distinctions, and a direct comparison is detailed in Figures 3, S4, and S5. To ensure that *s*-SPR and *t*-SPR encompass the same radiation range, the relationship between p and T is set as $p = T\beta c$ with the same harmonic order (see Note S5). It is worth noting that the evanescent field of a moving electron experiences exponential decay with increasing transverse distance, i.e., d_{Bohr}, and the proximity of the electron trajectory to the grating surface d plays a pivotal role.[50] In general, closer distances result in stronger interactions. However, this distance is constrained by experimental resolution to prevent direct electron impact on the structure for *s*-SPR.

In contrast, *t*-SPR exhibits robustness to variations in d. As the separation d increases, both *s*-SPR and *t*-SPR experience a reduction in intensity, but their rates of decline differ significantly. The intensity of *s*-SPR decreases exponentially toward zero as d reaches 3 mm, as illustrated in Figure 3A. On the other hand, *t*-SPR shows only a marginal decrease over the same distance, as depicted in Figures 3B (logarithmic scale) and S6 (linear scale). This disparity arises from their distinct excitation mechanisms. The intensity observed at the same radiation frequency f is influenced by the strength of the evanescent field from the source electron at frequency f_e. Specifically, for *t*-SPR, this is characterized by $d_{\mathrm{Bohr}}(f_e = f - mf_m)$, whereas for *s*-SPR, it is

$d_{\mathrm{Bohr}}(f_e = f)$. The characteristic length $d_{\mathrm{Bohr}}(f - mf_m)$ is significantly longer than $d_{\mathrm{Bohr}}(f)$, rendering *t*-SPR relatively insensitive to variations in the electron-grating separation. This feature alleviates the constraints typically associated with electron interactions within the near field.[64] Additionally, we compare the radiation angle distributions for *s*-SPR and *t*-SPR in Figures 3C and 3D by tuning β and reveal that normal emission $(\theta = 90^\circ)$ consistently occurs at f_m with varying β for *t*-SPR. This consistency is attributed to the fact that the radiation frequency f_m remains steadfast along the f axis, regardless of variations in β, and is accompanied by a corresponding wavenumber of $k_x = 0$. This feature highlights a potential application in frequency-locked light sources.[7,65]

Alongside its (1) strong robustness to electron-grating separation, *t*-SPR also offers two key advantages: enhanced reconfigurability and efficient energy management. (2) Reconfigurability and adaptability: *t*-SPR offers significant advantages in terms of reconfigurability compared to *s*-SPR. In *s*-SPR, the emission characteristics are primarily determined by the electron energy and the fixed spatial grating. The system lacks flexibility in adjusting these parameters once the grating is fabricated. Conversely, *t*-SPR provides a highly adaptable platform. The TG enables reconfiguration by adjusting several parameters: the modulation period T, the amplitude A (see Note S7 and Figure S7), and the modulation waveform $W(t)$, as shown in Figure 3E and beyond.[66] This flexibility allows for fine-tuning the interaction between the electrons and the time-varying field, offering enhanced control over the emission characteristics. The ability to adjust these parameters holds significant promise for developing advanced active free-electron light sources. (3) Enhanced energy transfer and amplification: in *s*-SPR, spatial grating operates as a passive system, strictly adhering to the principles of energy conservation. The role of the spatial grating is to convert evanescent waves, which are carried by electrons, into propagating waves within the spatial domain. The total energy within the system originates solely from the electrons, and there are no additional mechanisms for amplifying the energy. In contrast, *t*-SPR utilizing a TG functions as an active system. It does not strictly adhere to the conventional energy conservation constraints within the system. Instead, *t*-SPR can introduce external energy through temporal modulation. This modulation allows energy to be transferred from the temporal modulation to the electron-photon interaction, effectively sidestepping traditional energy conservation limitations. As a result, *t*-SPR can harness an additional energy channel, leading to significant enhancements in radiation intensity.

When periodic modulations are properly configured, the system exhibits amplification at specific frequencies, notably at $(2N+1)f_m/2$, where N is an integer. Adjusting the electron energy to $\beta = 0.23$ places the interaction point within the momentum gap (see Note S3 and Figure S2), inducing amplification. Ideal square waveforms, used throughout this study to illustrate *t*-SPR, have discontinuities that hinder the observation of this amplification effect. In order to address this, smooth transitions are introduced to create continuous waveforms $W(t)$ for all modulation types (sawtooth, square, triangular, and sinusoidal) (see Note S2). As shown in Figure 3E, the system exhibits amplification for all modulation types at normalized frequencies like 0.5, 1.5, 2.5, etc., consistent with recent photonic time crystal light emission findings.[46] Amplification may also arise from both the evanescent wave of the moving electron and *t*-iSPR, with their overlap causing amplified waves to leak into the vacuum and complicating *t*-SPR identification. Proper simulation time control is crucial to capture the *t*-SPR spectra and avoid masking from multiple amplification effects. As an active amplification mechanism, *t*-SPR shows potential for on-chip electron accelerators, enabling precise phase matching between the electron beam and *t*-SPR wave.[67–69]

Potential experiments to observe *t*-SPR

This study combines theoretical analysis with electromagnetic simulations to validate the concept of *t*-SPR. The proposed method is highly versatile, with no strict constraints on the modulation waveform, amplitude, frequency, or type of electron source, significantly improving experimental feasibility and broadening the range of potential setups. Various techniques for generating the TG have been explored in the literature,[40,41,51,70–74] with detailed comparisons provided in Table 1. For electron sources, options such as pencils, sheets, and hollow electron beams—commonly used in traditional SPR-based devices—are viable.[58,59,63] Electron microscopes, with their excellent collimation and manipulation capabilities, are particularly well suited for this application.[14,15,75,76] Additionally, artificial structures like slit waveguides can simulate electron evanescent waves,[11,12,56] expanding the possibilities for *t*-SPR experimentation. In experimental setups, achieving simultaneous and dynamic modulation of both material properties and the electron source is crucial for observing *t*-SPR. Two feasible approaches are proposed in Note S8 and Figure S8.

It is important to note that the TG concept is similar to, but distinct from, photonic time crystals. TG allows broad tuning by temporally modulating material properties at the working frequency (i.e., designed radiation frequency f) without constraints on the modulation frequency f_m. Experimental studies show that temporal modulation introduces Floquet frequency harmonics,[31,72,73] e.g., f = 196 THz (1,530 nm) with f_m = 1 MHz.[72] In contrast, photonic time crystals require ultrafast modulation frequencies near the working frequency and rely on creating a momentum gap for amplification. Achieving this experimentally is challenging, and the highest frequencies for metasurfaces are currently 871 and 1,742 MHz for working and modulation, respectively.[44] For initial *t*-SPR verification, amplification effects can be neglected to relax modulation frequency constraints.

DISCUSSION

In summary, our theoretical predictions reveal that *t*-SPR can be effectively achieved by a free electron moving above a simple TG. *t*-SPR emerges as a highly versatile platform thanks to its reliance on temporal modulation. Unlike traditional methods, *t*-SPR exhibits remarkable resilience to variations in the electron-to-grating distance, significantly easing the stringent requirements typically associated with near-field electron excitation in *s*-SPR. The amplification effect observed within the momentum gap of the TG highlights the potential of *t*-SPR for groundbreaking applications. This includes the development of

Table 1. Potential approaches to achieve TG

Material platform	Nonlinear materials[31,36]	Graphene[45,51,77–79]	Metasurface[44,74]	Transmission lines[37,80,81]
Mechanism	nonlinear Kerr effect	tunable Fermi level	reconfigurable metasurface	capacitance (inductance) modulation
Working frequency (designed radiation frequency)	infrared visible (~ 100 THz)	THz infrared (GHz–THz)	microwaves (MHz–GHz)	radio waves (kHz–MHz)
Modulation frequency	MHz–THz	~10 GHz	MHz	MHz
Waveform	sin/cos[31,a] square[72,a]	sin/cos[45,a,77] square[51,78]	sin/cos[44,a,74] square[73,a,82,a]	sin/cos[80,a,81,a]

[a]Experimental work.

advanced on-chip light sources and innovative electron accelerators.

Our study emphasizes the critical role of achieving high-speed modulation for the TG and addresses the implications of its finite thickness, as detailed in Note S9 and Figure S9. Similar to conventional *s*-SPR, which utilizes a transmission grating, *t*-SPR can be detected in both the upper and lower half-spaces. The radiation directions outlined in Equation 6 guide the detection. By highlighting these factors, we underscore the potential of *t*-SPR as a groundbreaking and practical approach for advancing the development of time-varying materials and integrated photonic and electronic devices. Our findings pave the way for future experimental research and technological innovations, particularly in the domain of free-electron radiation.

METHODS

Simulation methods

In this study, we utilized the transient solver in the commercial software COMSOL to validate the *t*-SPR. The current density induced by a moving electron is described by the equation $\mathbf{J}(x,z,t) = \hat{\mathbf{x}}qv_e\delta(z-d)\delta(x-v_et)$, where q is the electron charge and v_e is its velocity. In the frequency domain, the corresponding expression for the current density becomes $\mathbf{J}(x,z,\omega) = \hat{\mathbf{x}}q\delta(z-d)e^{-jk_{xe}x}$, where $k_{xe} = \omega_e/v_e$ and $k_{xe}^2 + k_{z0}^2 = (\omega_e/c)^2$. To simulate the motion of the moving electron, we employ a phase-delayed dipole array. The separation between adjacent dipoles is denoted as Δx ($\Delta x \ll \lambda$), with each dipole having a phase delay of $\Delta x k_{xe}$. In the time-domain simulation, a Gaussian wave packet is used to model the dipole array's excitation: $f(t) = A_0e^{-\frac{(t-t_0)^2}{2\sigma^2}}\cos(2\pi f_0 t)$, where A_0 is the amplitude, f_0 is the central frequency, t_0 represents its position on the time axis, and σ controls the wave packet's temporal width. To accurately capture the broadband nature of the source electron, σ is chosen to be sufficiently small. The simulation domain is divided into two regions: the vacuum and the TG. The source electron moves above the TG surface at a distance d. A scattering boundary condition is applied at the edges of the domain to absorb scattered waves and minimize reflection artifacts. Frequency-domain results are obtained through Fourier transform analysis, with a detection line configured to capture the radiation spectrum emitted by the dipole array. Additional details can be found in Note S2.

Energy band calculation for TG

A bulk TG with a time-periodically varying permittivity $\varepsilon_r(t)$ can be represented by a Fourier series due to its periodic nature. The Fourier series expansion of the permittivity is given by

$$\varepsilon_r(t) = \sum_m \varepsilon_m e^{jm\Omega t}, \quad \text{(Equation 8)}$$

where $m = 0, \pm1, \pm2, \cdots$, and Ω is the angular frequency of the time modulation. To solve the wave equation, we apply the Bloch-Floquet theorem, which allows the electric field $E(t)$ to be expressed as a Fourier series expansion:

$$E(t) = \sum_n e_n e^{j(\omega+n\Omega)t}, \quad \text{(Equation 9)}$$

where $n = 0, \pm1, \pm2, \cdots$, and ω is the base angular frequency. By substituting Equations 8 and 9 into Maxwell's equations, we obtain the following relation:

$$k_0^2c^2\sum_n e_n e^{jn\Omega t} - (\omega+n\Omega+m\Omega)^2\sum_m\sum_n e_n e_m e^{j(n+m)\Omega t} = 0, \quad \text{(Equation 10)}$$

where k_0 is the wave vector in the absence of the time-periodic modulation and c is the speed of light in vacuum. The detailed derivation and further explanation can be found in Note S3.

RESOURCE AVAILABILITY

Lead contact

Requests for further information and resources should be directed to and will be fulfilled by the lead contact, Lin Wu (lin_wu@sutd.edu.sg).

Materials availability

This study did not generate new unique materials.

Data and code availability

Any additional information required to reanalyze the data reported in this paper is available from the lead contact upon request.

ACKNOWLEDGMENTS

This work was funded by the Singapore University of Technology and Design Start-Up Research Grant SRG SMT 2021 169 and Kickstarter Initiative (SKI)

SKI 2021-02-14 and SKI 2021-04-12; the National Research Foundation Singapore via grant nos. NRF2021-QEP2-02-P03, NRF2021-QEP2-03-P09, and NRF-CRP26-2021-0004; and Ministry of Education Singapore MOE-T2EP50223-0001. The authors thank all members of the lab for their support.

AUTHOR CONTRIBUTIONS

Conceptualization, J.-F.Z. and L.W.; simulation, J.-F.Z. and A.N.; investigation, J.-F.Z., A.N., and Y.F.; writing—original draft, J.-F.Z., A.N., Y.F., and L.W.; writing—review & editing, J.-F.Z., A.N., Y.F., W.Z., Z.S., X. Wang, Z.-W.Z., C.-H.D., X. Wei, P.B., C.E.P., C.-W.Q., and L.W.; funding acquisition, L.W.; resources, L.W.; supervision, C.-W.Q. and L.W.

DECLARATION OF INTERESTS

The authors declare no competing interests.

SUPPLEMENTAL INFORMATION

Supplemental information can be found online at https://doi.org/10.1016/j.newton.2025.100023.

Received: August 31, 2024
Revised: December 15, 2024
Accepted: January 31, 2025
Published: February 27, 2025

REFERENCES

1. Smith, S.J., and Purcell, E.M. (1953). Visible light from localized surface charges moving across a grating. Phys. Rev. *92*, 1069.
2. Leavitt, R.P., Wortman, D.E., and Morrison, C.A. (1979). The orotron–a free-electron laser using the smith-purcell effect. Appl. Phys. Lett. *35*, 363–365.
3. Nanni, E.A., Huang, W.R., Hong, K.H., Ravi, K., Fallahi, A., Moriena, G., Miller, R.J.D., and Kärtner, F.X. (2015). Terahertz-driven linear electron acceleration. Nat. Commun. *6*, 8486.
4. Urata, J., Goldstein, M., Kimmitt, M.F., Naumov, A., Platt, C., and Walsh, J.E. (1998). Superradiant smith-purcell emission. Phys. Rev. Lett. *80*, 516–519.
5. Su, Z., Xiong, B., Xu, Y., Cai, Z., Yin, J., Peng, R., and Liu, Y. (2019). Manipulating cherenkov radiation and smith–purcell radiation by artificial structures. Adv. Opt. Mater. *7*, 1801666.
6. Roques-Carmes, C., Kooi, S.E., Yang, Y., Rivera, N., Keathley, P.D., Joannopoulos, J.D., Johnson, S.G., Kaminer, I., Berggren, K.K., and Soljačić, M. (2023). Free-electron–light interactions in nanophotonics. Appl. Phys. Rev. *10*.
7. Korbly, S.E., Kesar, A.S., Sirigiri, J.R., and Temkin, R.J. (2005). Observation of frequency-locked coherent terahertz smith-purcell radiation. Phys. Rev. Lett. *94*, 054803.
8. Wang, Z., Yao, K., Chen, M., Chen, H., and Liu, Y. (2016). Manipulating smith-purcell emission with babinet metasurfaces. Phys. Rev. Lett. *117*, 157401.
9. Su, Z., Cheng, F., Li, L., and Liu, Y. (2019). Complete control of smith-purcell radiation by graphene metasurfaces. ACS Photonics *6*, 1947–1954.
10. Kaminer, I., Kooi, S., Shiloh, R., Zhen, B., Shen, Y., López, J., Remez, R., Skirlo, S., Yang, Y., Joannopoulos, J., et al. (2017). Spectrally and spatially resolved smith-purcell radiation in plasmonic crystals with short-range disorder. Phys. Rev. X *7*, 011003.
11. Jing, L., Lin, X., Wang, Z., Kaminer, I., Hu, H., Li, E., Liu, Y., Chen, M., Zhang, B., and Chen, H. (2021). Polarization shaping of free-electron radiation by gradient bianisotropic metasurfaces. Laser Photon. Rev. *15*, 2000426.
12. Jing, L., Wang, Z., Lin, X., Zheng, B., Xu, S., Shen, L., Yang, Y., Gao, F., Chen, M., and Chen, H. (2019). Spiral field generation in smith-purcell radiation by helical metagratings. Research (Wash D C) *2019*. https://doi.org/10.34133/2019/3806132.
13. Zhang, Z.W., Zhu, J.F., Du, C.H., Gao, F., Han, F.Y., and Liu, P.K. (2023). Chiral plasmons enable coherent vortex smith–purcell radiation. Laser Photon. Rev. *17*, 2200420.
14. Yang, Y., Massuda, A., Roques-Carmes, C., Kooi, S.E., Christensen, T., Johnson, S.G., Joannopoulos, J.D., Miller, O.D., Kaminer, I., and Soljačić, M. (2018). Maximal spontaneous photon emission and energy loss from free electrons. Nat. Phys. *14*, 894–899.
15. Yang, Y., Roques-Carmes, C., Kooi, S.E., Tang, H., Beroz, J., Mazur, E., Kaminer, I., Joannopoulos, J.D., and Soljačić, M. (2023). Photonic flatband resonances for free-electron radiation. Nature *613*, 42–47.
16. Engheta, N. (2023). Four-dimensional optics using time-varying metamaterials. Science *379*, 1190–1191.
17. Fante, R. (1971). Transmission of electromagnetic waves into time-varying media. IEEE Trans. Antenn. Propag. *19*, 417–424.
18. Koufidis, S.F., Koutserimpas, T.T., Monticone, F., and McCall, M.W. (2024). Enhanced scattering from an almost-periodic optical temporal slab. Phys. Rev. *110*, L041501.
19. Koufidis, S.F., Koutserimpas, T.T., and McCall, M.W. (2023). Temporal analog of bragg gratings. Opt. Lett. *48*, 4500–4503.
20. Koutserimpas, T.T. (2022). Parametric amplification interactions in time-periodic media: coupled waves theory. JOSA B *39*, 481–489.
21. Moussa, H., Xu, G., Yin, S., Galiffi, E., Ra'di, Y., and Alù, A. (2023). Observation of temporal reflection and broadband frequency translation at photonic time interfaces. Nat. Phys. *19*, 863–868.
22. Ortega-Gomez, A., Lobet, M., Vázquez-Lozano, J.E., and Liberal, I. (2023). Tutorial on the conservation of momentum in photonic time-varying media. Opt. Mater. Express *13*, 1598–1608.
23. Ginzburg, V.L., and Tsytovich, V. (1979). Several problems of the theory of transition radiation and transition scattering. Phys. Rep. *49*, 1–89.
24. Ginzburg, V.L. (1982). Transition radiation and transition scattering. Phys. Scripta *1982*, 182–191.
25. Barsukov, K., and Grigor'eva, N.Y. (1996). Radiation in a semi-infinite nonstationary inhomogeneous medium. J. Tech. Phys. *41*, 706–709.
26. Mkrtchyan, A.R., Potylitsyn, A.P., Kocharyan, V.R., and Saharian, A.A. (2016). Transition radiation on a dynamic periodic interface. Phys. Rev. E *93*, 022117.
27. Mkrtchyan, A.R., Parazian, V., and Saharian, A. (2018). Transition radiation on a superlattice in finite thickness plate generated by two acoustic waves. J. Instrum. *13*, C01032.
28. Mkrtchyan, A., Parazian, V., and Saharian, A. (2020). Transition radiation of electron bunches on acoustic superlattices. Armenian Journal of Physics *13*, 70–83.
29. Bacot, V., Labousse, M., Eddi, A., Fink, M., and Fort, E. (2016). Time reversal and holography with spacetime transformations. Nat. Phys. *12*, 972–977.
30. Sounas, D.L., and Alù, A. (2017). Non-reciprocal photonics based on time modulation. Nat. Photonics *11*, 774–783.
31. Guo, X., Ding, Y., Duan, Y., and Ni, X. (2019). Nonreciprocal metasurface with space–time phase modulation. Light Sci. Appl. *8*, 123.
32. Pacheco-Peña, V., and Engheta, N. (2020). Temporal aiming. Light Sci. Appl. *9*, 129.
33. Horsley, S.A.R., and Pendry, J.B. (2023). Quantum electrodynamics of time-varying gratings. Proc. Natl. Acad. Sci. USA *120*, e2302652120.
34. Horsley, S.A.R., and Pendry, J.B. (2024). Traveling wave amplification in stationary gratings. Phys. Rev. Lett. *133*, 156903.
35. Pacheco-Peña, V., and Engheta, N. (2020). Antireflection temporal coatings. Optica *7*, 323–331.

36. Tirole, R., Vezzoli, S., Galiffi, E., Robertson, I., Maurice, D., Tilmann, B., Maier, S.A., Pendry, J.B., and Sapienza, R. (2023). Double-slit time diffraction at optical frequencies. Nat. Phys. *19*, 999–1002.

37. Galiffi, E., Xu, G., Yin, S., Moussa, H., Ra'di, Y., and Alù, A. (2023). Broadband coherent wave control through photonic collisions at time interfaces. Nat. Phys. *19*, 1703–1708.

38. Lee, K., Son, J., Park, J., Kang, B., Jeon, W., Rotermund, F., and Min, B. (2018). Linear frequency conversion via sudden merging of meta-atoms in time-variant metasurfaces. Nat. Photonics *12*, 765–773.

39. Oue, D., Ding, K., and Pendry, J.B. (2022). Čerenkov radiation in vacuum from a superluminal grating. Phys. Rev. Res. *4*, 013064.

40. Yin, S., Galiffi, E., and Alù, A. (2022). Floquet metamaterials. ELight *2*, 1–13.

41. Galiffi, E., Tirole, R., Yin, S., Li, H., Vezzoli, S., Huidobro, P.A., Silveirinha, M.G., Sapienza, R., Alù, A., and Pendry, J.B. (2022). Photonics of time-varying media. Adv. Photonics *4*, 014002.

42. Lustig, E., Sharabi, Y., and Segev, M. (2018). Topological aspects of photonic time crystals. Optica *5*, 1390–1395.

43. Lyubarov, M., Lumer, Y., Dikopoltsev, A., Lustig, E., Sharabi, Y., and Segev, M. (2022). Amplified emission and lasing in photonic time crystals. Science *377*, 425–428.

44. Wang, X., Mirmoosa, M.S., Asadchy, V.S., Rockstuhl, C., Fan, S., and Tretyakov, S.A. (2023). Metasurface-based realization of photonic time crystals. Sci. Adv. *9*, eadg7541.

45. Galiffi, E., Wang, Y.T., Lim, Z., Pendry, J.B., Alù, A., and Huidobro, P.A. (2020). Wood anomalies and surface-wave excitation with a time grating. Phys. Rev. Lett. *125*, 127403.

46. Dikopoltsev, A., Sharabi, Y., Lyubarov, M., Lumer, Y., Tsesses, S., Lustig, E., Kaminer, I., and Segev, M. (2022). Light emission by free electrons in photonic time-crystals. Proc. Natl. Acad. Sci. USA *119*, e2119705119.

47. Zurita-Sánchez, J.R., Halevi, P., and Cervantes-González, J.C. (2009). Reflection and transmission of a wave incident on a slab with a time-periodic dielectric function $\varepsilon(t)$. Phys. Rev. *79*, 053821.

48. van den Berg, P.M. (1973). Smith–purcell radiation from a line charge moving parallel to a reflection grating. JOSA *63*, 689–698.

49. Chaturvedi, P., Hsu, K.H., Kumar, A., Fung, K.H., Mabon, J.C., and Fang, N.X. (2009). Imaging of plasmonic modes of silver nanoparticles using high-resolution cathodoluminescence spectroscopy. ACS Nano *3*, 2965–2974.

50. Lu, S., Nussupbekov, A., Xiong, X., Ding, W.J., Png, C.E., Ooi, Z.E., Teng, J.H., Wong, L.J., Chong, Y., and Wu, L. (2023). Smith–purcell radiation from highly mobile carriers in 2d quantum materials. Laser Photon. Rev. *17*, 2300002.

51. Kim, K.H., and O, K.H. (2024). Graphene plasmonic time crystals. Physica Rapid Research Ltrs. *18*, 2400116.

52. Pacheco-Peña, V., and Engheta, N. (2020). Effective medium concept in temporal metamaterials. Nanophotonics *9*, 379–391.

53. Koutserimpas, T.T., and Fleury, R. (2020). Electromagnetic fields in a time-varying medium: exceptional points and operator symmetries. IEEE Trans. Antenn. Propag. *68*, 6717–6724.

54. Konakhovych, D., Sniezek, D., Warmusz, O., Black, D.S., Zhao, Z., England, R.J., and Szczepkowicz, A. (2021). Internal smith-purcell radiation and its interplay with cherenkov diffraction radiation in silicon–a combined time and frequency domain numerical study. Preprint at arXiv. https://doi.org/10.48550/arXiv.2207.07048.

55. García de Abajo, F.J. (2010). Optical excitations in electron microscopy. Rev. Mod. Phys. *82*, 209–275.

56. Xi, S., Chen, H., Jiang, T., Ran, L., Huangfu, J., Wu, B.I., Kong, J.A., and Chen, M. (2009). Experimental verification of reversed cherenkov radiation in left-handed metamaterial. Phys. Rev. Lett. *103*, 194801.

57. Chen, H., and Chen, M. (2011). Flipping photons backward: reversed cherenkov radiation. Mater. Today *14*, 34–41.

58. Duan, Z., Tang, X., Wang, Z., Zhang, Y., Chen, X., Chen, M., and Gong, Y. (2017). Observation of the reversed cherenkov radiation. Nat. Commun. *8*, 14901.

59. Liu, F., Xiao, L., Ye, Y., Wang, M., Cui, K., Feng, X., Zhang, W., and Huang, Y. (2017). Integrated cherenkov radiation emitter eliminating the electron velocity threshold. Nat. Photonics *11*, 289–292.

60. Linhart, J.G. (1955). Čerenkov radiation of electrons moving parallel to a dielectric boundary. J. Appl. Phys. *26*, 527–533.

61. Gaxiola-Luna, J.G., and Halevi, P. (2021). Temporal photonic (time) crystal with a square profile of both permittivity $\varepsilon(t)$ and permeability $\mu(t)$. Phys. Rev. B *103*, 144306.

62. Gaxiola-Luna, J., and Halevi, P. (2023). Growing fields in a temporal photonic (time) crystal with a square profile of the permittivity $\varepsilon(t)$. Appl. Phys. Lett. *122*.

63. Ye, Y., Liu, F., Wang, M., Tai, L., Cui, K., Feng, X., Zhang, W., and Huang, Y. (2019). Deep-ultraviolet smith–purcell radiation. Optica *6*, 592–597.

64. Kong, J.A. (1975). Theory of Electromagnetic Waves (New York: Wiley-Interscience).

65. Zhu, J.F., Du, C.H., Li, F.H., Bao, L.Y., and Liu, P.K. (2019). Free-electron-driven multi-frequency terahertz radiation on a super-grating structure. IEEE Access *7*, 181184–181190.

66. Sharabi, Y., Lustig, E., and Segev, M. (2021). Disordered photonic time crystals. Phys. Rev. Lett. *126*, 163902.

67. Zhang, D., Zeng, Y., Tian, Y., and Li, R. (2023). Coherent free-electron light sources. Photonics Insights *2*, R07.

68. Chlouba, T., Shiloh, R., Kraus, S., Brückner, L., Litzel, J., and Hommelhoff, P. (2023). Coherent nanophotonic electron accelerator. Nature *622*, 476–480.

69. Zhang, D., Zeng, Y., Bai, Y., Li, Z., Tian, Y., and Li, R. (2022). Coherent surface plasmon polariton amplification via free-electron pumping. Nature *611*, 55–60.

70. Asgari, M.M., Garg, P., Wang, X., Mirmoosa, M.S., Rockstuhl, C., and Asadchy, V. (2024). Photonic time crystals: Theory and applications. Preprint at arXiv. https://doi.org/10.48550/arXiv.2404.04899.

71. Saha, S., Segal, O., Fruhling, C., Lustig, E., Segev, M., Boltasseva, A., and Shalaev, V.M. (2023). Photonic time crystals: a materials perspective. Opt. Express *31*, 8267–8273.

72. Sisler, J., Thureja, P., Grajower, M.Y., Sokhoyan, R., Huang, I., and Atwater, H.A. (2024). Electrically tunable space–time metasurfaces at optical frequencies. Nat. Nanotechnol. *19*, 1491–1498.

73. Zhang, L., Chen, X.Q., Liu, S., Zhang, Q., Zhao, J., Dai, J.Y., Bai, G.D., Wan, X., Cheng, Q., Castaldi, G., et al. (2018). Space-time-coding digital metasurfaces. Nat. Commun. *9*, 4334.

74. Wang, X., Garg, P., Mirmoosa, M.S., Lamprianidis, A.G., Rockstuhl, C., and Asadchy, V.S. (2025). Expanding momentum bandgaps in photonic time crystals through resonances. Nat. Photonics *19*, 1–7.

75. Wang, K., Dahan, R., Shentcis, M., Kauffmann, Y., Ben Hayun, A., Reinhardt, O., Tsesses, S., and Kaminer, I. (2020). Coherent interaction between free electrons and a photonic cavity. Nature *582*, 50–54.

76. Dahan, R., Nehemia, S., Shentcis, M., Reinhardt, O., Adiv, Y., Shi, X., Be'er, O., Lynch, M.H., Kurman, Y., Wang, K., and Kaminer, I. (2020). Resonant phase-matching between a light wave and a free-electron wavefunction. Nat. Phys. *16*, 1123–1131.

77. Li, W., Chen, B., Meng, C., Fang, W., Xiao, Y., Li, X., Hu, Z., Xu, Y., Tong, L., Wang, H., et al. (2014). Ultrafast all-optical graphene modulator. Nano Lett. *14*, 955–959.

78. Wilson, J., Santosa, F., Min, M., and Low, T. (2018). Temporal control of graphene plasmons. Phys. Rev. B *98*, 081411.

79. Phare, C.T., Daniel Lee, Y.H., Cardenas, J., and Lipson, M. (2015). Graphene electro-optic modulator with 30 ghz bandwidth. Nat. Photonics *9*, 511–514.

80. Reyes-Ayona, J., and Halevi, P. (2015). Observation of genuine wave vector (k or β) gap in a dynamic transmission line and temporal photonic crystals. Appl. Phys. Lett. *107*.

81. Reyes-Ayona, J.R., and Halevi, P. (2016). Electromagnetic wave propagation in an externally modulated low-pass transmission line. IEEE Trans. Microw. Theor. Tech. *64*, 3449–3459.

82. Wang, S.R., Dai, J.Y., Zhou, Q.Y., Ke, J.C., Cheng, Q., and Cui, T.J. (2023). Manipulations of multi-frequency waves and signals via multi-partition asynchronous space-time-coding digital metasurface. Nat. Commun. *14*, 5377.